1   **Full-Scale Evaluation of Geogrid Reinforced Thin Flexible Pavements**

3   **Sarah R. Jersey, P.E.**
4   Civil Engineer
5   U.S. Army Corps of Engineers, Risk Management Center
6   1000 Liberty Avenue
7   Pittsburgh, PA 15222
8   (412) 395-7183 (phone)
9   Sarah.R.Jersey@usace.army.mil

11   **Jeb S. Tingle, P.E. (corresponding author)**
12   Research Civil Engineer
13   U.S. Army Engineer Research and Development Center
14   3909 Halls Ferry Road
15   Vicksburg, MS 39180
16   (601) 634-2467 (phone)
17   Jeb.S.Tingle@usace.army.mil

19   **Gregory J. Norwood, P.E.**
20   Research Civil Engineer
21   U.S. Army Engineer Research and Development Center
22   3909 Halls Ferry Road
23   Vicksburg, MS 39180
24   (601) 634-3373 (phone)
25   Gregory.J.Norwood@usace.army.mil

27   Jayhyun Kwon, Ph.D., P.E.
28   Tensar International Corporation
29   2500 Northwinds Parkway, Suite 500
30   Alpharetta, Georgia 30009
31   (770)-344-2133 (Phone)
32   JKwon@tensarcorp.com

34   Mark Wayne, Ph.D., P.E.
35   Tensar International Corporation
36   2500 Northwinds Parkway, Suite 500
37   Alpharetta, Georgia 30009
38   (770)-344-2133 (Phone)
39   MWayne@tensarcorp.com

41   Submission Date: 01 August 2011

43   **Word Count:** 3767
44   **Figure Count:** 9
45   **Table Count:** 6
46   **Equivalent Word Count:** 7517

1
2 **ABSTRACT:**
3 A full-sale test section was constructed and trafficked at the U.S. Army Engineer Research and
4 Development Center to evaluate the performance of a geogrid used for base reinforcement in a
5 thin, flexible pavement. Three test items consisting of a geogrid-reinforced test item and two
6 unreinforced control test items were constructed under controlled conditions. The test
7 pavements were subjected to accelerated trafficking to evaluate the relative performance of the
8 various pavement structures. Permanent surface deformations and pavement stiffness were
9 measured periodically throughout traffic testing. The results of the study showed that the
10 geogrid reinforced pavement significantly improved the performance relative to the unreinforced
11 control pavements. Results were used to develop traffic benefit ratios and effective base course
12 structural coefficients which provide a means for comparing the various pavement structures.
13
14

1 **INTRODUCTION**
2 Transportation professionals are presented with the challenge of building and maintaining
3 growing infrastructure systems under the constraints of shrinking budgets. The competing
4 demands of minimizing costs and maximizing performance are a key issue for designers and
5 maintainers at the federal, state and local levels. The inclusion of geosynthetics in flexible
6 pavement structures for base reinforcement has long been accepted as a means of reducing costs
7 and/or extending pavement service life. As new products enter the market, designers are forced
8 to speculate concerning the performance benefits of these products when specifying them. Many
9 research efforts have documented and attempted to quantify the performance benefit of biaxial
10 geogrids (1-9). Most researchers agree that the inclusion of geogrids can result in reduced
11 aggregate base thickness requirements or extended service live of the pavement. However, very
12 little research has been completed regarding the full-scale testing of new triaxial geogrid
13 products.
14   The objective of the research described in this study was to evaluate the performance benefits
15 of an emerging triaxial geogrid product in thin, flexible pavements. This was accomplished
16 through construction and traffic testing of a full-scale test section containing three different test
17 items. The test section included a geogrid-reinforced test item and two unreinforced control test
18 items for performance comparison. The performance of the test items was evaluated in terms of
19 the development of permanent surface deformation, or rutting, under simulated truck traffic. The
20 performance data were used to establish performance characteristics of the new geogrid product
21 under realistic conditions for a typical low-volume flexible pavement system.
22
23 **TEST SECTION DESIGN AND LAYOUT**
24 A profile view of the test section's pavement structural design is shown in FIGURE 1. Three
25 different pavement profiles were tested, each consisting of an 8-ft-wide by 50-ft-long test area.
26 One test item was reinforced with a new geogrid product installed at the base-subgrade interface
27 (Item A) and two items were constructed without reinforcement (Items B and C). Test Items A
28 and B were designed to directly compare the effect of the geogrid reinforcement in similar
29 pavement sections, while Items A and C were designed to evaluate the equivalency of the
30 geogrid reinforcement compared to an extra inch of asphalt concrete. The subgrade for each test
31 item was consisted of 28 in. of high-plasticity clay (CH) with a target subgrade California
32 Bearing Ratio (CBR) of 3% placed over a compacted silt (ML) soil with an in situ CBR of 8-
33 10%. Once the subgrade was prepared, the geogrid product was installed in Item A. The
34 subgrade was overlain with an 8-in. thick aggregate base course consisting of crushed limestone.
35 The limestone was covered with a thin asphalt concrete surface course. Items A and B were
36 constructed with a 2-in. thick asphalt concrete surface layer, while Item C was constructed with a
37 3-in. thick asphalt concrete surface layer. The test items were constructed simultaneously to
38 minimize the variability of the as-constructed properties of the different test items. The ERDC's
39 open-ended pavement test facility prevented moisture intrusion due to rainfall during testing.
40
41 **MATERIAL CHARACTERIZATION**
42 **Subgrade**
43   The subgrade was constructed using locally available high plasticity clay (CH) shown in
44 FIGURE 2. The CH soil was composed of 98% fines passing the #200 sieve. The liquid limit,
45 plastic limit, and plasticity index were determined to be 83, 29, and 54, respectively following
46 the procedures described in ASTM C 856-02-07 [10]. The soil classifies as a high-plasticity clay
47 (CH) in the Unified Soil Classification System (USCS) and an A-7-6(63) according the

1   AASHTO procedure [12]. When processed to a uniform moisture and density condition, the CH
2   material produces a uniform undrained shear strength profile.   Based on historical experience, a
3   moisture content of approximately 41.0% was selected to obtain the 3 CBR strength required for
4   the subgrade. Modified Proctor tests were performed in accordance with ASTM D 1557-07--07,
5   Method A Modified [11]. At the target moisture content of 41.0%, the maximum dry density
6   was 78.4 pcf.
7
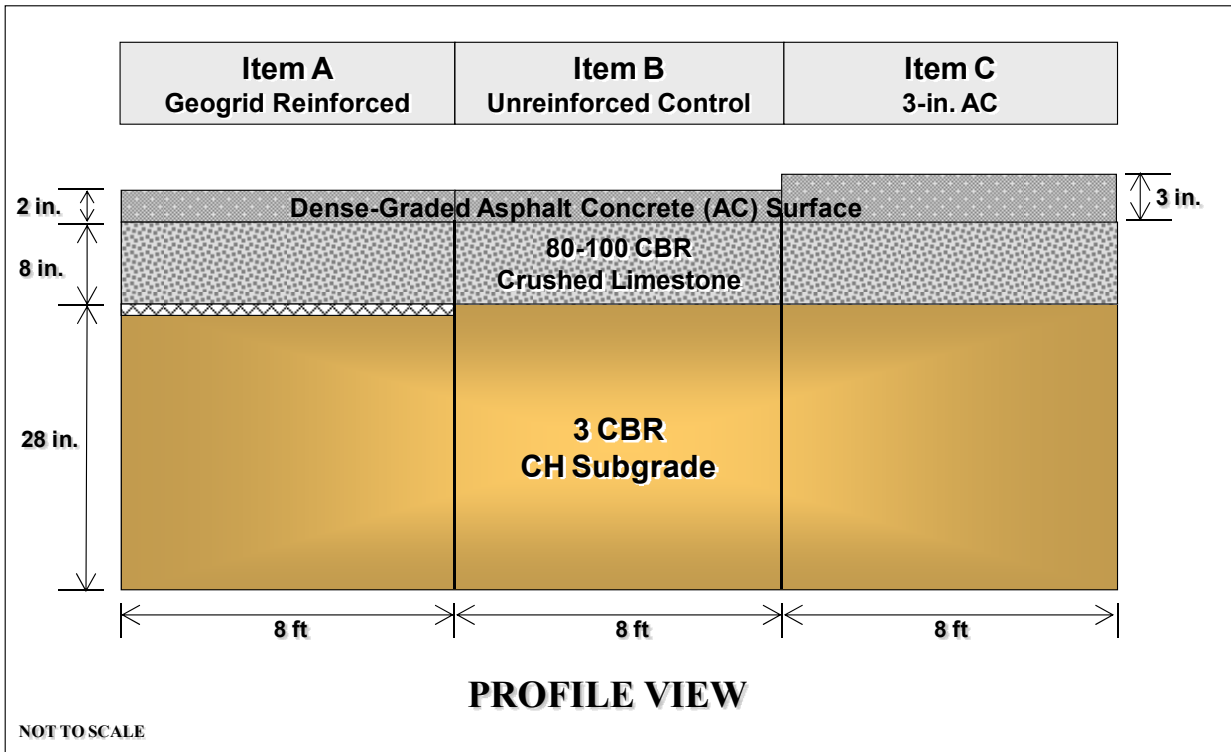
8
9   FIGURE 1 Profile View of Test Section (not to scale).
10
11   **Base course**
12   The aggregate base course was constructed using crushed limestone with the gradation shown in
13   FIGURE 2. The crushed limestone was composed of 61% gravel, 32% sand, and 7% non-plastic
14   fines passing the #200 sieve. The coefficients of curvature (C_c), and uniformity (C_u) were 3.55
15   and 49.33, respectively. The crushed limestone was classified as a poorly graded silty gravel
16   (GP-GM) in the Unified Soil Classification System (USCS) and an A-1-a according the
17   AASHTO procedure [12]. Modified proctor tests were performed in accordance with ASTM D
18   1557-07-07, Method C Modified [11]. At the optimum moisture content of 4.3%, the maximum
19   dry density was 148.9 pcf.
20
21   **Asphalt concrete surface course**
22   The asphalt concrete (AC) surface material in this test section was selected as representative of a
23   highway mix for Mississippi. Laboratory tests were performed to characterize the asphalt
24   concrete. The aggregate gradation was measured using the wet sieve method [12]. TABLE 1
25   summarizes the gradation of the aggregates used in the asphalt concrete surface and the results of
26   the Marshall mix design tests. The mix used in this test meets the Asphalt Institute guidance for
27   Marshall mix design of medium-volume roads (10,000-1,000,000 ESALs) [18].

U. S. STANDARD SIEVE OPENING IN INCHES
4 3 2 1½ 1 ¾ ½ ⅜ 3 4 6 8 10 14 16 20 30 40 50 70 100 140 200

U. S. STANDARD SIEVE NUMBERS

HYDROMETER

PERCENT FINER BY WEIGHT

PERCENT COARSER BY WEIGHT

GRAIN SIZE IN MILLIMETERS

GRAVEL		SAND			SILT OR CLAY	
COARSE	FINE	COARSE	MEDIUM	FINE		

SAMPLE NO.	MATERIAL	CLASSIFICATION	NAT W%	LL	PL	PI	GRADATION CURVES	
1	Vicksburg Buckshot	High Plasticity Clay (CH)		79	23	56	PROJECT **Geogrid Test Section**	
2	Crushed Limestone	Gravel (GP-GM)				NP	SOURCE **Waterways Experiment Station**	
							DATE **June 2008**	

1
2 **FIGURE 2 Gradation of base and subgrade materials.**

1
2

TABLE 1 Properties of the Asphalt Concrete Surface

US Standard Sieve Size	Diameter (in.)	Percent Finer
1 in.	1 .00	100.0
3/4 in.	0.75	99.3
1/2 in.	0.50	99.0
3/8 in.	0.375	94.6
No. 4	0.187	59.2
No. 8	0.0937	34.4
No. 16	0.0394	24.2
No. 30	0.0234	19.0
No. 50	0.0117	11.1
No. 100	0.0049	7.8
No. 200	0.0029	5.6
Marshall Mix Design Results		
Marshall Stability (lb) AASHTO T 245 [13]	3359	
Marshall Flow (0.01 in) AASHTO T 245 [13]	12.7	
Tensile Strength Ratio (%)	104	
Specific Gravity AASHTO T 209 [14]	2.425	
Asphalt Content (%)	4.87	
Percent Air Voids (%) AASHTO T 269 [15]	4.48	

3
4 **Geogrids**
5 The geogrid, denoted GGA, was a new triaxial geogrid product and consists of a series of
6 concentric triangles, forming a series of concentric hexagons. The geogrids are composed of a
7 black high-density polypropylene. The reported junction efficiency was 93% with an aperture
8 stability of 3.6 kg-cm/deg at 5.0 kg-cm. The radial stiffness at 0.5% strain was reported as 300
9 kN/m.
10
11 **PAVEMENT CHARACTERIZATION**
12 A series of tests were performed to characterize the as-constructed properties of the pavement
13 materials. During construction, dry density and moisture content were obtained for each
14 subsurface pavement layer using a nuclear moisture-density device as described by ASTM D
15 3017-04 [16]. These values provide a means of assessing the uniformity of the constructed
16 layers as well as the comparative value of the various pavement layers.
17 In-field CBR values were obtained following the standards set forth in ASTM D4429-04
18 [17]. The in-field CBR data show subgrade strengths ranging from 2.8 to 3.1%. Additionally, a
19 series of tests were performed using the Dynamic Cone Penetrometer (DCP) to characterize the
20 strength of the unbound pavement layers following the procedures described by ASTM D 6951-
21 09 [18]. Measured values of the DCP index (millimeters of penetration per hammer blow) were
22 converted to CBR strength using the relationship developed by Webster et al. [19]. The DCP
23 testing indicated subgrade strengths of 3.5 to 4.0 CBR. The results of the DCP tests showed that
24 the high quality limestone base was constructed to a strength of 100 CBR. The transition from

1 base to subgrade was observed around a depth of 8 inches for all three test items. The as-built
2 properties of the subgrade and base course are summarized in TABLE 2.
3
4   **TABLE 2 Summary of as-built properties of base and subgrade materials.**

	Item A	Item B	Item C
Test	**GGA**	**Control**	**3 in. AC**
CH Subgrade Properties			
Wet Density (pcf)	113.8	114.0	112.9
Dry Density (pcf)	83.6	83.5	83.0
Nuclear Moisture (%)	36.1	36.1	36.2
Oven-Dried Moisture (%)	37.0	37.9	38.9
$CBR_{In-Field}$ (%)	3.1	2.9	2.8
CBR_{DCP} (%)	3.3	4.0	3.5
In situ vane shear (psi)	15.2	15.5	15.9
Crushed Limestone Base Properties			
Wet Density (pcf)	153.2	153.8	154.6
Dry Density (pcf)	148.8	149.7	150.1
Nuclear Moisture (%)	2.9	2.7	3.0
Oven-Dried Moisture (%)	2.3	2.1	1.4
$CBR_{In-Field}$ (%)	91	100+	100+
CBR_{DCP} (%)	100+	100+	100+
Thickness (in.)	7.42	8.09	7.90

5
6   Falling Weight Deflectometer (FWD) tests were performed on each test item after
7 construction of the AC surface. FWD results were analyzed in terms of the Impulse Stiffness
8 Modulus (ISM), the ratio of the applied load to the measured plate deflection. The average post
9 construction ISM values for Items A, B, and C were 240, 220, and 310 kips/in., respectively.
10 The minor variability observed in the initial stiffness results for Items A and B is likely due to
11 the inherent variability in the heterogeneous nature of pavement materials and minor structural
12 differences between the as-constructed test items. The improved initial stiffness of Item C is due
13 to the presence of an additional inch of asphalt concrete surface.
14
15 **TRAFFIC TESTING**
16 Traffic testing of the test items was accomplished using the ERDC's Heavy Vehicle Simulator
17 (HVS-A). Traffic testing of Item B (Control) was accomplished using a dual-wheel single axle
18 loaded to a nominal load of 10,000 lb (FIGURE 3 (a)). The loaded contact pressure associated
19 with the dual-wheel single axle load was approximately 88 psi with a recorded tire pressure of
20 120 psi. Traffic testing of the remaining test items was accomplished using a dual-wheel tandem
21 axle loaded to a nominal load of 20,000 lb (FIGURE 3 (b)) and recorded tire pressures of 120 psi.
22 The dual-wheel tandem axle loading essentially applied two distinct load pulses, each with a
23 loaded contact pressure of approximately 88 psi.   The tandem axle was used to provide double
24 the traffic coverage in a single pass of the load carriage and better simulates the actual truck
25 configurations. Adverse effects associated with trafficking using tandem axle rather than the
26 single axle were considered nominal.

1

2
3   (a)   (b)
4   **FIGURE 3 Axles used during trafficking of geogrid reinforced pavements**
5   **(a) dual-wheel single axle, (b) dual-wheel tandem axle.**
6
7   The test items were subjected to a normally distributed bi-directional traffic load, as shown
8   schematically in FIGURE 4. This represents the wander in a typical traffic lane, as observed by
9   Timm and Priest [20].   The load carriage traverses the test section longitudinally at each 1-in.
10   offset index location. Thus, the extent of the lateral wander associated of this traffic pattern is
11   approximately 3 feet. Traffic loading was applied over a 50-foot length along each test item.
12   Data collection was performed along the inner 40-ft section of the traffic lane to avoid the
13   transition zone at each end of the test lane. The failure criterion for these pavements was a 1-in.
14   surface rut, including any upheaval adjacent to the traffic lane. Items B and C were trafficked
15   beyond that level to ensure that adequate pavement response and performance data were
16   obtained. Unfortunately, traffic on Item A was stopped prematurely due to the inadvertent
17   flooding of the test item by a burst water pipe from an adjacent building. The HVS-A test
18   chamber was enclosed and the ambient temperature was held at 77°F +/- 2°F throughout testing
19   to minimize the effect of the temperature dependent response of the asphalt concrete surface.
20
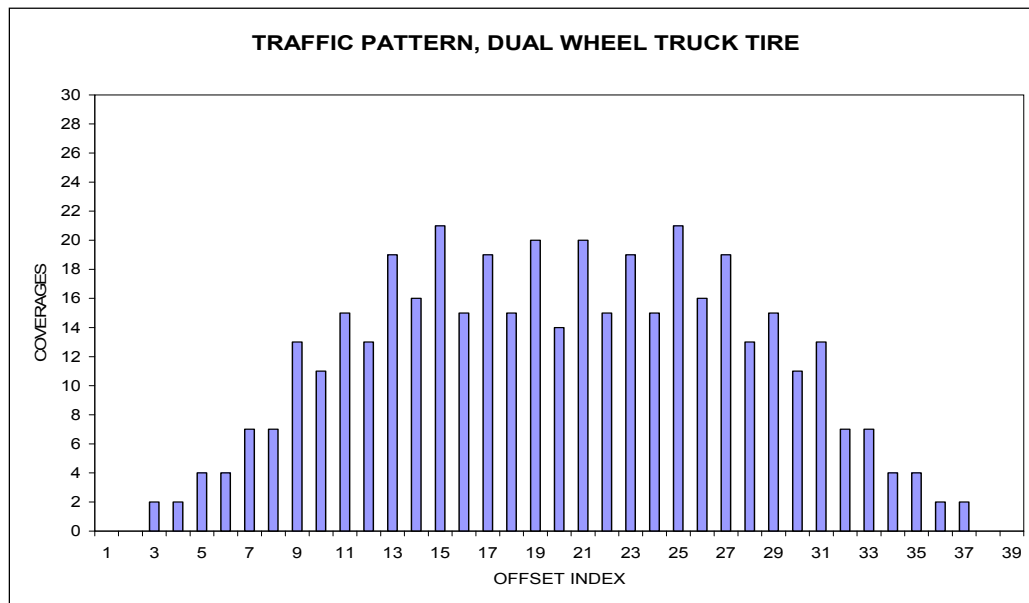
21
22   **FIGURE 4 Lateral wander pattern used for application of traffic**
23

1 **RESULTS**
2 **Rutting and Permanent Surface Deformation**
3 Rut depth is an indicator of a pavement's structural performance, particularly in thin pavements
4 where subgrade failure is expected to govern rather than fatigue of the asphalt concrete surface
5 layer. In this study, the pavement was considered failed at a rut depth of 1 in. due to the
6 resulting decrease in pavement serviceability. Rutting was measured at five locations along the
7 length of each test item (Stations 9, 12.5, 25, 37.5, and 43) at selected traffic intervals throughout
8 traffic testing. Rut depth measurements were performed at the centerline and at a one foot offset
9 on both sides of the center line at each of these stations. The average of these values was used to
10 as the rut depth at the station.
11   The average rutting measured at various traffic levels is shown in FIGURE 5. This figure
12 indicates that the onset of rutting occurred more rapidly in Items B and C (the unreinforced
13 control items) than in the geogrid-reinforced pavement (Item A). Further, these data indicate that
14 that the pavement service life of the geogrid-reinforced test item exceeded that of the
15 unreinforced test items.
16   A test item was considered failed when 50% of the test item exceeded a rut depth of 1 in.
17 This is consistent with the reliability of 50% used in the initial pavement design assumptions.
18 The traffic levels at which the various levels of rutting are summarized in TABLE 3. This table
19 also includes the traffic levels at which several other pertinent rut levels were exceeded. This
20 analysis is based upon the average rut depth at 3 of the 5 stations exceeding the rutting
21 thresholds. These data support the observations discussed previously: the unreinforced control
22 with the 2-in. AC surface (Item B) sustained the least traffic, followed by the unreinforced item
23 with the 3-in. AC surface (Item C), and then the geogrid-reinforced Item A.
24   In addition to measurements of rutting at discrete locations, the longitudinal pavement profile
25 was surveyed at a number of traffic levels during testing.   These profiles report permanent
26 surface deformation and should not be confused with rutting measurements as they do not
27 include the upheaval component of the rut. The longitudinal profiles show that deformations
28 began to increase rapidly at one or more locations in each test item corresponding to the weakest
29 points in the pavement system. Pavement failure propagates outward from these initial locations,
30 inducing failure in the adjacent areas at an accelerated rate. The propagation of permanent
31 deformations for Items A and B are shown in FIGURE 6.
32
33   **TABLE 3 Summary of ESALs at Various Levels of Surface Deformation**

Test Item	Treatment	0.25 in.	0.50 in.	0.75 in.	1.0 in.
Item A	GGA	19,300	100,000+	100,000+	100,000+
Item B	2-in. AC Control	1,800	8,100	9,500	13,000
Item C	3-in. AC Control	4,220	16,300	24,500	27,870

34
35
36

Applied ESALs
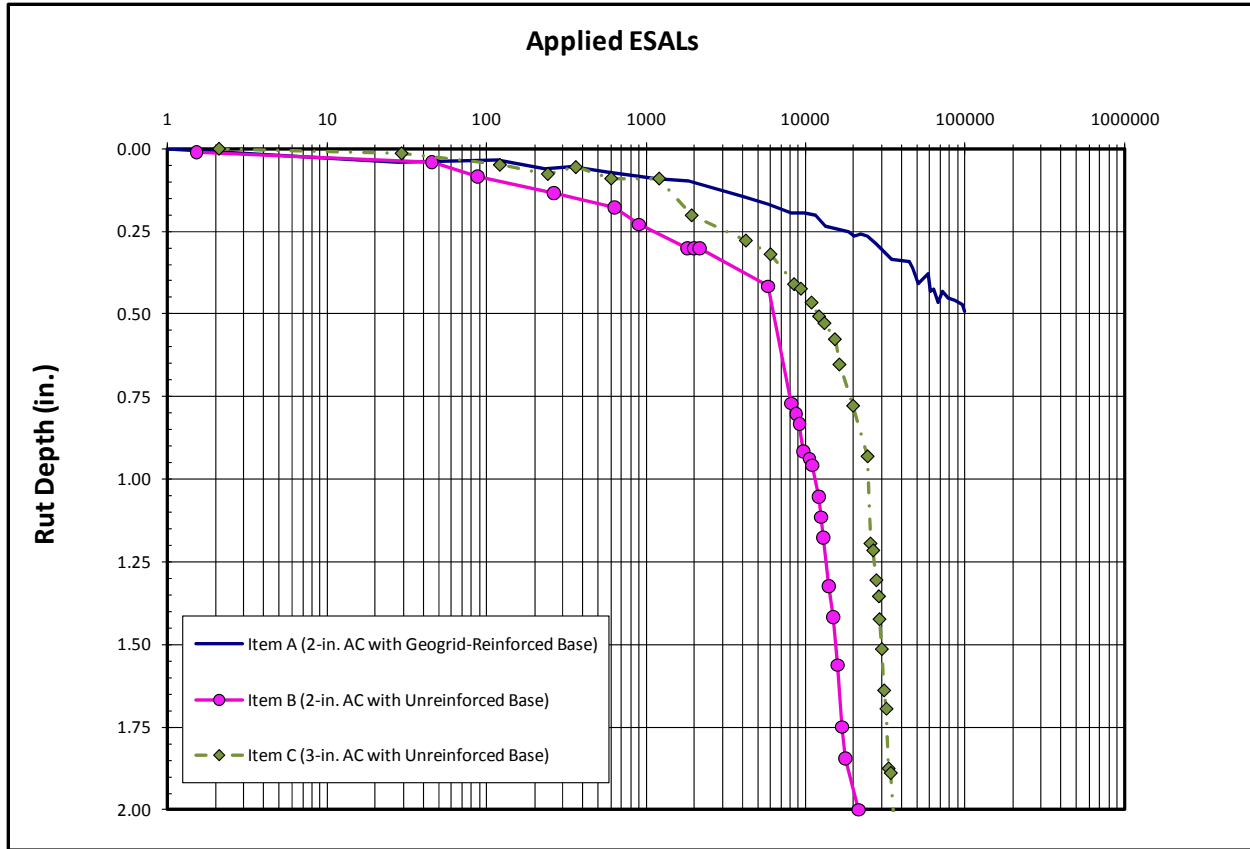
FIGURE 5 Accumulation of rutting at selected traffic levels.
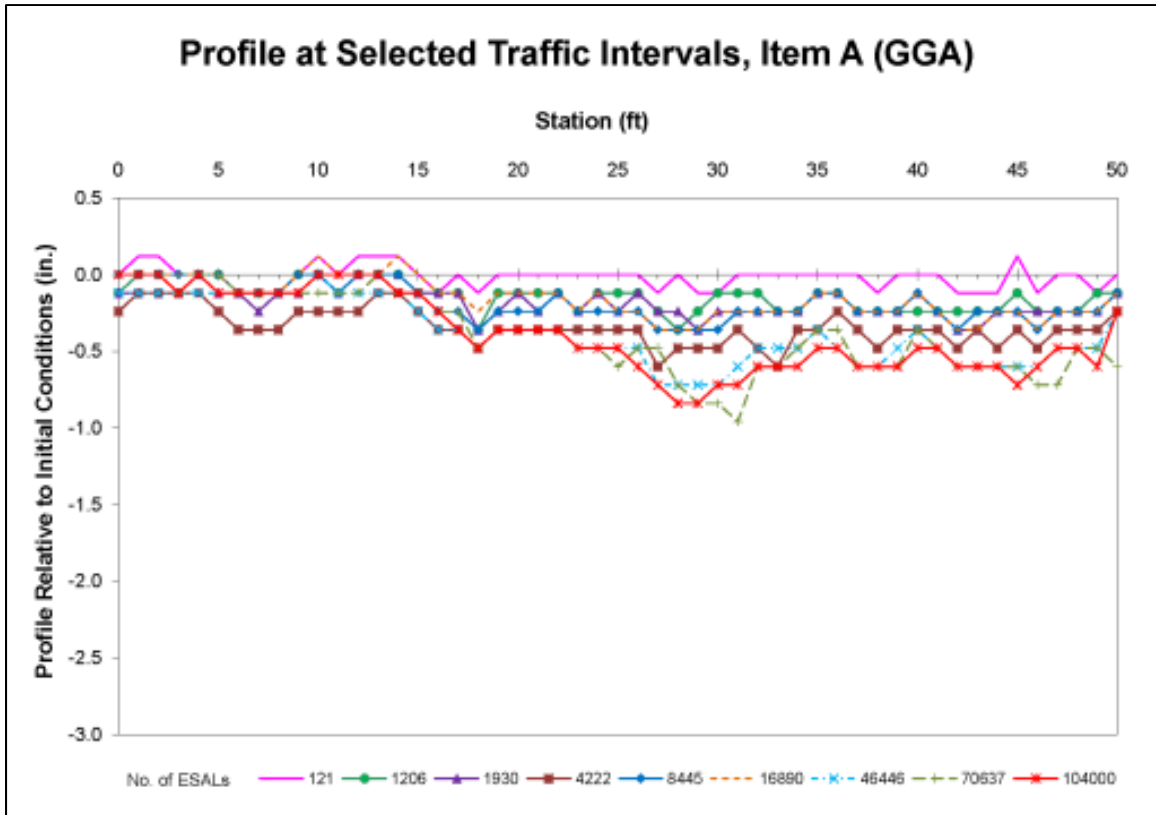
(a) Permanent Surface Deformation of Item A
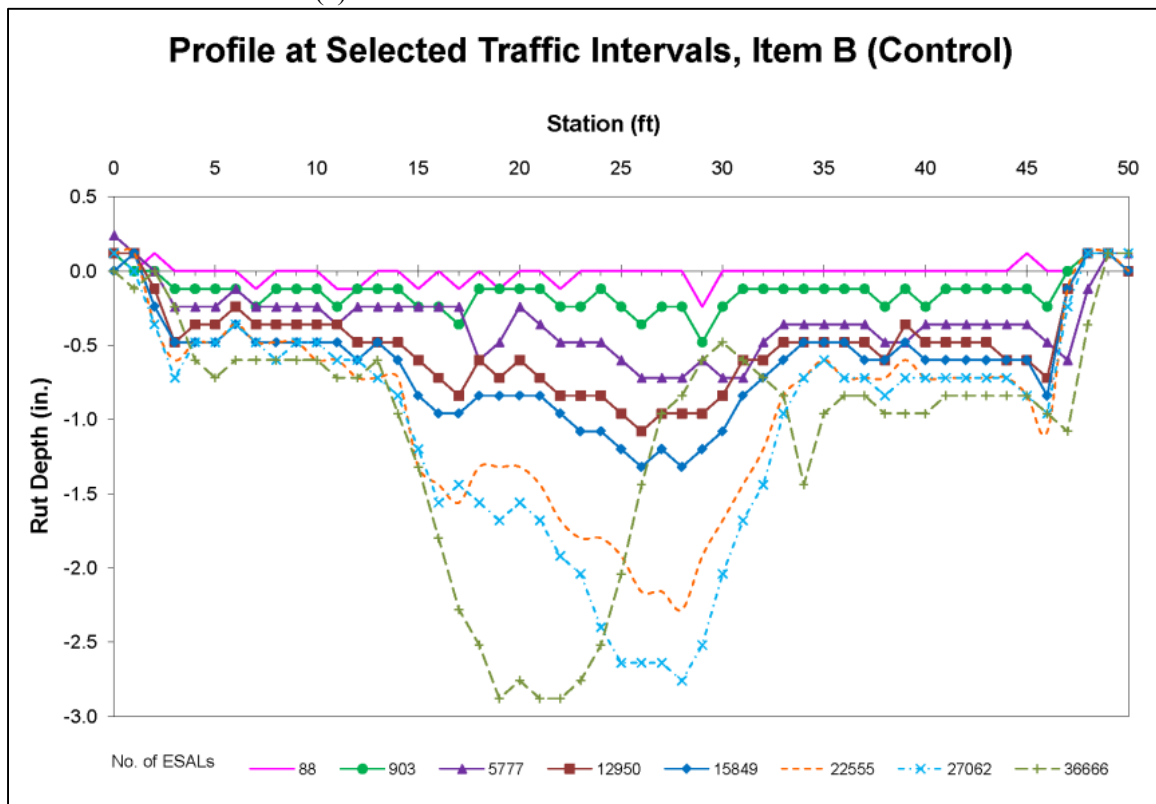
(b) Permanent Surface Deformation of Item B

FIGURE 6 Propagation of failure along pavement centerline for selected test items (a) Item A, (b) Item B.

Post-Test Forensics

After trafficking, post-test forensics were performed to characterize the pavement layers. The asphalt concrete surface was removed in a 3-ft-long, 5-ft-wide section at Stations 12 and 30 as representative locations within the traffic lane. In-field CBR, DCP, nuclear density, and oven-dried moisture tests were performed at the top of the base course layer. The granular base and geogrid were then excavated, and CBR, DCP, nuclear density, and oven-dried moisture contents were performed on the subgrade surface. The post-test forensics data are presented in TABLE 4.

In general, there was not a significant increase in the dry density of the subgrade. The dry density of the aggregate base course materials reduced from the levels measured prior to the onset of traffic. This was particularly prominent in those areas where shear flow had initiated indicating damage to the pavement system.

Subsurface rutting behavior at these stations was significantly different, as shown in FIGURE 7. FIGURE 7 (a) shows minimal rutting in the base course of Item A and no distresses were observed in the subgrade. It should be noted that trafficking of this item was halted after 100,000 ESALs due to inadvertent flooding of the test area. The absence of measurable rutting in the base or subgrade may be a result of halting traffic prior to exceeding the 1-in. failure criteria along 50% of the length of the test item. FIGURE 7 (b) shows the subsurface rutting shown in Item B. The base thickness is reduced directly beneath centerline of the traffic lane while excessive aggregate material in the upheaval area indicates shear flow in the base layer. FIGURE 7 (c) shows evidence of more moderate shear flow in Item C (3-in. AC).

Stiffness

The stiffness of each test item was characterized through interpretation of the FWD results. Data were analyzed in terms of the Impulse Stiffness Modulus (ISM), a normalization of the applied load by the resulting deflection at the load plate. At each traffic interval, ISM values were calculated at seven locations, Stations 12.5, 17, 21, 25, 29, 33, and 37.5. FIGURE 8 shows the degradation of the pavement stiffness with a corresponding increase in the applied traffic.

At the onset of testing, ISM values ranged from 200-250 kips/in. for Item A, 100-200 kips/in. for Item B, and 200-250 kips/in. for Item C. Under sustained traffic loading, values dropped as low as 50 kips/in. for Items B and C. In Item B, a significant drop in stiffness occurred between 2,000 and 10,000 ESALs. This corresponds to the onset of significant rutting which occurred at approximately 5,000. A similar loss of stiffness was observed during trafficking of Item C at a traffic level of approximately of 13,000 ESALs. It appears that the reduction in stiffness of Item A was significantly less than for the unreinforced sections; however, traffic was halted prior to reaching the 1-in. rut depth. Under sustained traffic beyond 100,000 ESALs the stiffness values would be expected to eventually drop to these reduced levels.

In addition, the base damage index (BDI) was computed as the difference between the D1 and D2 deflection measurements (deflection at the center of the plate and a 12-in. offset) as an indicator or the relative stiffness of the aggregate base course. FIGURE 9 shows a plot of the change in BDI with applied traffic for station 25, the midpoint location of the test items. As shown in the figure, the base stiffness values for the reinforced test item appear to be higher than those computed for the control item. There is a marked decrease in base stiffness for Item C after 10,000-13,000 ESALs, while Item A appears to retain its base stiffness. These data would support that the base stiffness was increased and maintained due to the mechanical reinforcement of the geogrid.

TABLE 4 Summary of Post-Test Forensic Results from Base Course

Test Item	Station 12						Station 30					
	Wheelpath			Shoulder			Wheelpath			Shoulder		
	CBR (%)	Dry Density (pcf)	Moisture Content (%)	CBR (%)	Dry Density (pcf)	Moisture Content (%)	CBR (%)	Dry Density (pcf)	Moisture Content (%)	CBR (%)	Dry Density (pcf)	Moisture Content (%)
CH Subgrade Post-Test Properties												
Item A	2.1	84.4	35.6	2.2	80.8	37.3	2.5	84.1	35.4	2.0	84.7	34.2
Item B	3.0	85.8	33.3	2.1	84.2	34.9	2.5	79.1	41.4	2.0	79.7	39.5
Item C	3.4	82.5	39.7	3.4	78.3	40.9	3.5	85.1	34.1	2.6	84.6	34.9
Crushed Limestone Base Post-Test Properties												
Item A	75	137.7	2.6	73	141.8	2.5	100+	145.3	3.1	100+	144.6	3.3
Item B	93	146.8	3.1	65	143.5	3.2	100+	152.4	2.8	47	146.0	3.0
Item C	100+	150.0	3.0	70	139.2	3.9	100+	150.1	2.9	53	143.7	3.5

(a)

(b)   (c)

**FIGURE 7 Pavement cross sections observed during post-traffic forensic investigations
(a) Item A, GGA; (b) Item B, 2-in. AC Control; and (c), Item C 3-in. AC Control.**

(a)
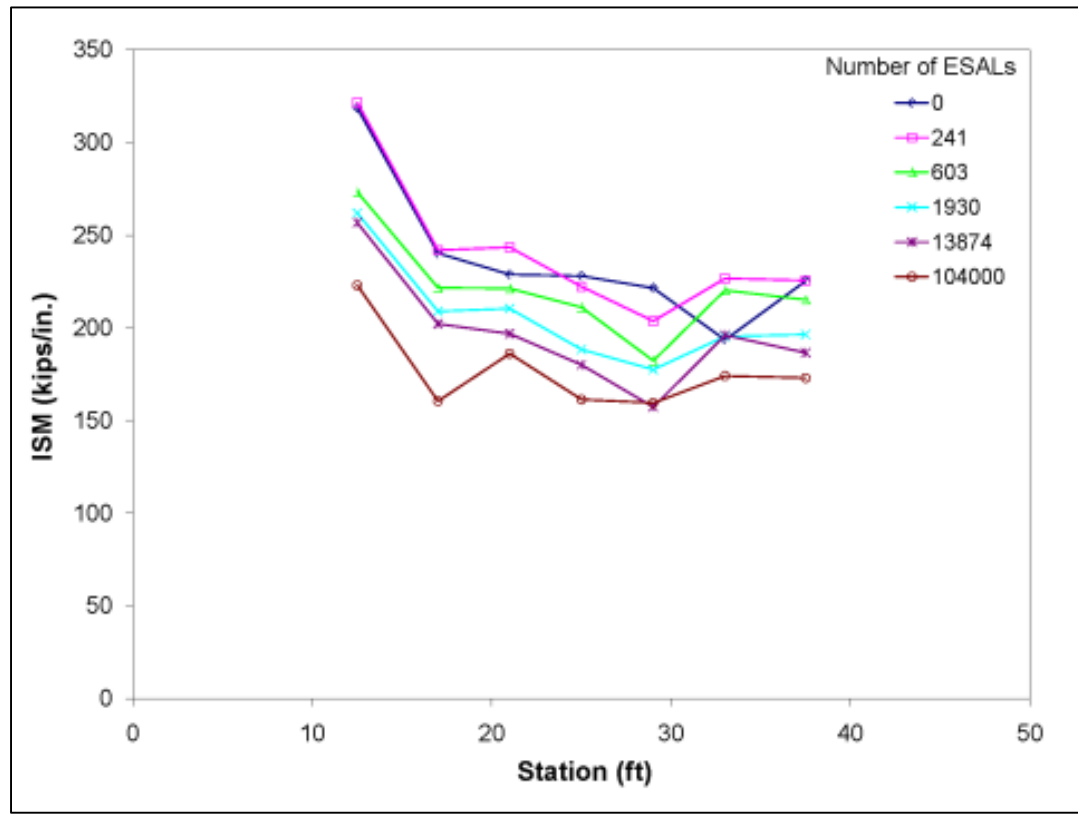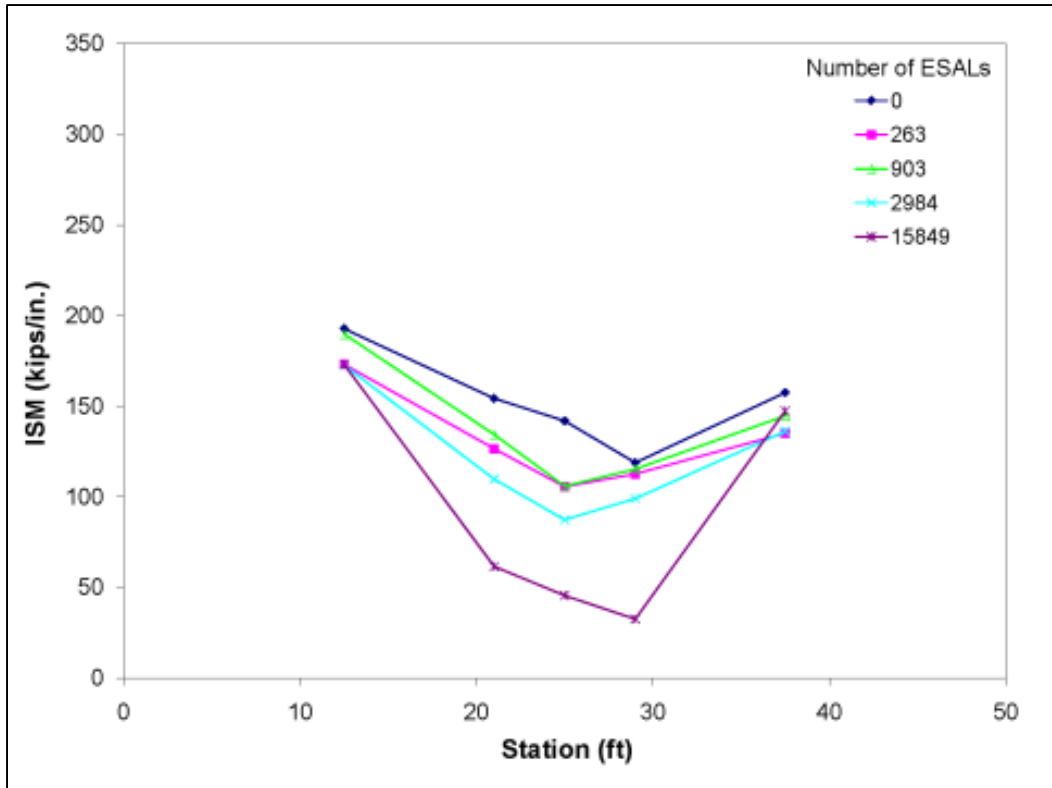
(c)
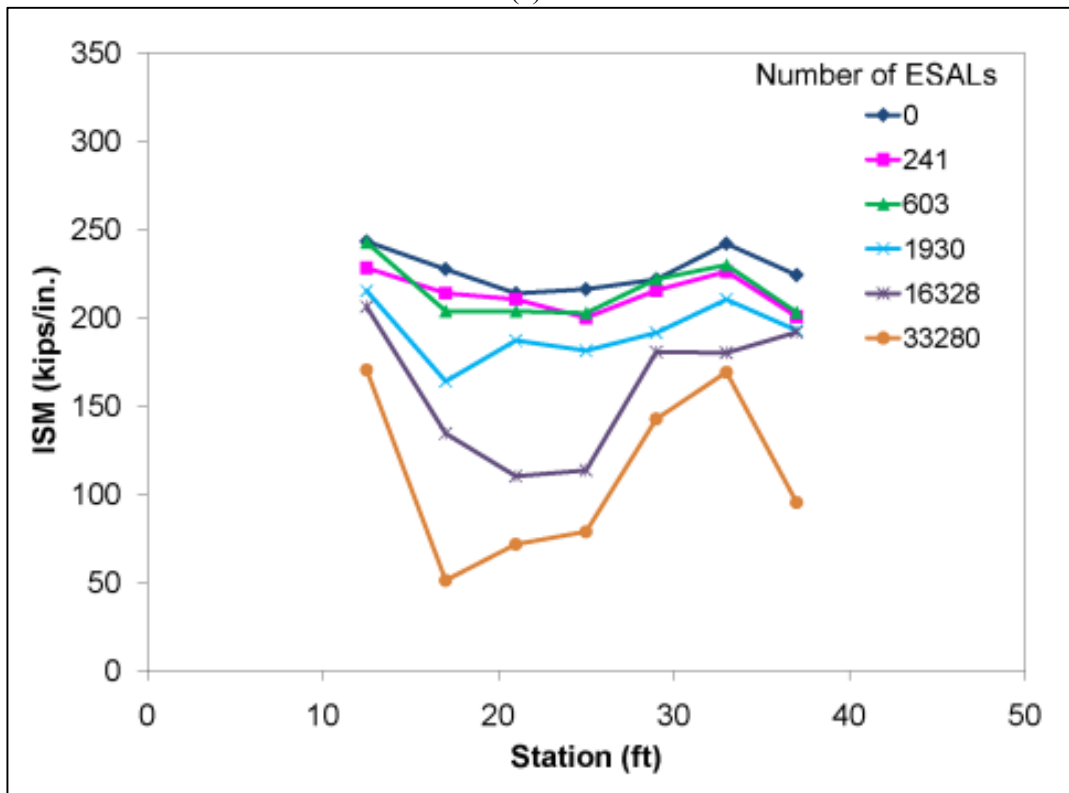
(d)

FIGURE 8 Degradation of pavement stiffness under applied traffic
(a) Item A, GGA; (b) Item B, 2-in. AC Control; and (c) Item C, 3-in. AC Control.

1
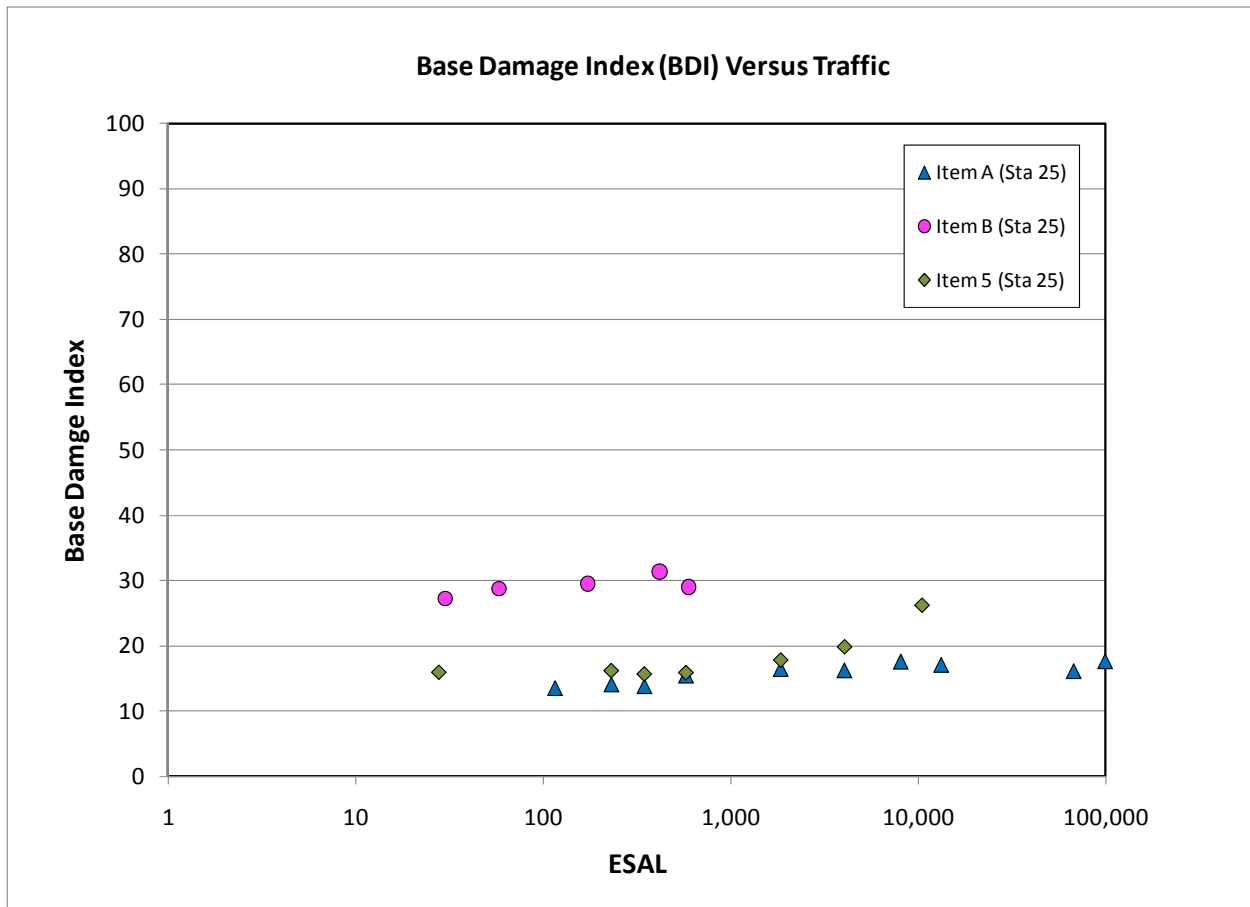
FIGURE 9 Comparison of Base Damage Index (BDI) versus applied traffic

Traffic Benefit Ratio

One method of quantifying the relative benefit of a geosynthetic within the pavement structure is
the Traffic Benefit Ratio (TBR). The TBR provides an index of the performance benefit of the
geosynthetic relative to an unreinforced pavement structure. The TBR values measured during
this study are summarized in TABLE 5. As noted previously, traffic was discontinued on Item A
after 100,000 ESALs due to flooding of the test area. For comparison purposes, a TBR for Item
A was computed based on the applied 100,000 ESALs for rut depths of 0.5, 0.75, and 1.0 in.
given that additional traffic on the test item to produce those rut depths would only result in
higher computed TBRs. Excessive TBR values, such as those computed for Item A, should not
be interpreted as evidence that the reinforced pavement will have an infinite lifespan. These
results merely highlight the improved performance of the geogrid relative to the unreinforced
control section rather than providing a multiplier for design purposes.

TABLE 5 Summary of Traffic Benefit Ratios (TBRs) at Various Rut Depths Relative to Control (Item C)

Test Item	Treatment	0.25 in.	0.50 in.	0.75 in.	1.0 in.
Item A[1]	GGA	11	12+	10+	7+
Item B	2-in. AC Control	1	1	1	1
Item C	3-in. AC Control	2	2	3	2

[1]Since traffic was forced to stop at 100,000 ESALs for Item A, the TBRs were computed based upon the applied 100,000 ESALs. Additional traffic to achieve the various rut levels would result in higher computed TBRs.

Effective Structural Capacity

The as-built pavement thicknesses and passes-to-failure were used to calculate an effective structural coefficient for the base course of the four test items using the AASHTO Design Pavement Design Guide. These values are summarized in TABLE 6. The effective base course structural coefficient represents an adjustment to the standard base course coefficient which accounts for the actual passes sustained by the test section and the actual base course thickness. Thus, the effective base course structural coefficient is higher for the geogrid reinforced pavement, Items A. These values were used to calculate an effective structural number. The effective structural number provides a better comparison when considering test items with varying thicknesses of asphalt concrete. Despite the fact that testing of Item A was not conducted to failure, the previous results clearly display a significant increase in structural capacity for that test item relative to its design values. Unfortunately the results cannot be quantified for an equal comparison to the remaining items, although it should be noted that the pavement withstood over 100,000 ESALs before reaching a 0.5-in. rut.

TABLE 6 Effect of Geosynthetic on Pavement Performance

	Item A[1] Geogrid	Item B Control	Item C 3 in. AC
Design Base Thickness (in.)	8	8	8
Design Structural Number	2	2	2.44
Design Passes to Failure	41,000	41,000	41,000
As-Built Asphalt Thickness (in.)	1.81	1.66	2.61
As-built Base Thickness (in.)	7.63	8.34	7.89
Passes-to-Failure	100,000+	13,000	27,870
Effective Base Coefficient	0.19+	0.11	0.09
Effective Structural Number	2.28+	1.62	1.85

[1]Since traffic was forced to stop at 100,000 ESALs for Item A, the effective base coefficient and effective structural number for Item A were computed based upon the applied 100,000 ESALs. Additional traffic to achieve the various rut levels would result in higher computed values of both parameters.

CONCLUSIONS

A full-scale test section was constructed and trafficked to evaluate the performance of geosynthetic reinforced thin asphalt pavements. The analysis of the results produced several conclusions regarding the benefit of incorporating geosynthetics into thin asphalt pavements:

1. The pavement test items were constructed in a uniform manner with minor variability between test items. The uniformity of construction allows meaningful comparisons between test items to be made.
2. The geogrid reinforced pavement section significantly improved the resistance to rutting compared to the unreinforced control test item.
3. The geogrid reinforced test item provided more resistance to rutting than did the 3-in. AC surfaced unreinforced control test item.
4. The initial stiffness of the reinforced test item was not a good indicator of performance. However, there was a noticeable drop in pavement stiffness accompanying the onset of surface rutting.
5. The computed traffic benefit ratios indicate that the geogrid used in this study should extend the service life of the pavement significantly.

ACKNOWLEDGEMENTS

REFERENCES

1. Kim, Woon-Hyung, T.B. Edil,C.H. Benson, and B.F. Tanyu. Structural Contribution of Geosynthetic-Reinforced Working Platforms in Flexible Pavement. In *Transportation Research Record 1936*, TRB, National Research Council, Washington, D.C., 2005, pp. 43-50.
2. Aran, Shirwan. Base Reinforcement with Biaxial Geogrid. In *Transportation Research Record 1975*, TRB, National Research Council, Washington, D.C., 2006, pp. 115-123.
3. Christopher, B.R., R.R. Berg, and S.W. Perkins. *Geosynthetic Reinforcements in Roadway Sections Report*. NCHRP Project 20-7 Task 112. TRB, National Research Council, Washington, D.C., 2001.
4. Barksdale, R., S. Brown, and F. Chan. *NCHRP Report 315: Potential Benefits of Geosynthetics in Flexible Pavement Systems*. TRB, National Research Council, Washington, D.C., 1989.
5. Haas, R., J.Walls, and R.G. Carroll. Geogrid Reinforcement of Granular Bases in Flexible Pavements. In *Transportation Research Record 1188*, TRB, National Research Council, Washington, D.C., 1988, pp. 19-27.
6. Al-Qadi, I.L., T.L. Brandon, R.J. Valentine, B.A. Lacina, and T.E. Smith. Laboratory Evaluation of Geosynthetic-Reinforced Pavement Sections. In *Transportation Research Record 1188*, TRB, National Research Council, Washington, D.C., 1988, pp. 25-31.
7. Perkins, S.W., and M. Ismeik. A Synthesis and Evalaution of Geosynthetic Reinforced Base Layers in Flexible Pavements: Part I. In *Geosynthetics International*, Vol. 4, No. 6, 1999, pp. 549-605.
8. Tingle, J.S., and S.R. Jersey. Empirical Design Methods for Geosynthetic-Reinforced Low-Volume Roads. In *Transportation Research Record 1989*, TRB, National Research Council, Washington, D.C., 2007, pp. 91-101.
9. Berg, R.R., B.R. Christopher, and S.W. Perkins. *Geosynthetic Reinforcement of the Aggregate Base/Subbase Courses of Flexible Pavement Structures*. GMA White Paper II. Geosynthetic Materials Association, Roseville, MN, 2000.
10. American Society for Testing and Materials (ASTM). 2004. *Standard test methods for classification of soils for engineering purposes (Unified Soil Classification System)*. Designation: D 2487-06. West Conshohocken, PA
11. American Society for Testing and Materials (ASTM). 2002. *Standard test methods for laboratory compaction characteristics of soil using modified effort*. Designation: D 1557-07. West Conshohocken, PA

1   12. Association of American Highway and Transportation Officials (AASHTO). 2006. *Standard Method*
2   *of Test for Sieve Analysis of Fine and Coarse Aggregates*, AASHTO T027-06, Washington, D.C.
3   13. Association of American Highway and Transportation Officials (AASHTO). 2004. *Standard Method*
4   *of Test for Resistance to Plastic Flow of Bituminous Mixtures Using Marshall Apparatus*, AASHTO
5   T245-97, Washington, D.C.
6   14. Association of American Highway and Transportation Officials (AASHTO). 2008. *Standard Method*
7   *of Test for Theoretical Maximum Specific Gravity and Density of Hot Mix Asphalt (HMA)*, AASHTO
8   T209-08, Washington, D.C
9   15. Association of American Highway and Transportation Officials (AASHTO). 2007. *Standard Method*
10   *of Test for Percent Air Voids in Compacted Dense and Open Asphalt Mixtures*, AASHTO T269-97,
11   Washington, D.C.
12   16. American Society for Testing and Materials (ASTM). 2004. *Standard test methods for water content*
13   *of soil and rock in place by nuclear methods (shallow depth)*. Designation: D 3017-04. West
14   Conshohocken, PA
15   17. American Society for Testing and Materials (ASTM). 2004. *Standard test method for CBR*
16   *(California Bearing Ratio) of soils in place*. Designation: D 4429-04. West Conshohocken, PA
17   18. American Society for Testing and Materials (ASTM) 2009. *Standard Test Method for Use of the*
18   *Dynamic Cone Penetrometer in Shallow Pavement Applications*. Designation: D 6951-09. West
19   Conshohocken, PA
20   19. Webster, S.L., R.W. Brown, and J.R. Porter. 1994. *Force projection site evaluation using the*
21   *electrical cone penetrometer (ECP) and the dynamic cone penetrometer (DCP)*. Technical Report
22   GL-94-17. Vicksburg, MS. U.S. Army Waterways Experiment Station.
23   20. Timm, D.H., and A. L. Priest. 2005. Wheel Wander at the NCAT Test Track, NCAT Report 05-02.
24   Auburn, AL.

25